High Performance Computing with Python

Final Report

Shuhei Watanabe

5171091

watanabs@informatik.uni-freiburg.de

July 30, 2021

Contents

1 Introduction **2**

2 Lattice Boltzmann method **3**
2.1 The Boltzmann transport equation (BTE) 3
2.2 Time-step update of the BTE 3
2.3 Boundary handling 4
2.3.1 Bounce-back from objects 5
2.3.2 Periodic boundary conditions (PBC) 5

3 Implementation **6**
3.1 Main routine 6
3.2 Parallel computation by MPI 6

4 Numerical results **10**
4.1 Validation experiments 10
4.1.1 Shear wave decay 10
4.1.2 Couette flow 13
4.1.3 Poiseuille flow 14
4.2 Lid-driven cavity 14

5 Conclusions **18**

1

Introduction

Large-scale physics experiments often require large budgets and it is hard to perform experiments with several different parameters. For this reason, many research has been performed to simulate real-world phenomenon. One of the phenomenon is the fluid flow. For example, fluid flow simulations allow us to deeply understand how the car body shape relates to the aerodynamic drag and to optimize the car design through the simulations with various designs rather than making real cars [1].

Such simulations require scheme to simulate the physical states at each time step and the lattice Boltzmann method (LBM) [2] is one of the well-known schemes for the fluid flow simulation method. LBM approximates the physical states of a myriad of microscopic particles, i.e. usually obtained by solving Navier-Stokes equation, by mesoscale physical states at each lattice grid. The physical states or **moments** are iteratively simulated based on the Maxwell velocity distribution function [3] and the fluid flow at each time step is derived from the moments.

The major advantages of LBM are the followings:

- **Simple implementation**: The governing equations of each moment is simple and the collision handling only considers the adjacent lattices.
- **Parallelization**: The parallelization scales well due to the local dynamics nature of LBM [4]

For those reasons, LBM is one of the most successful methods and we would like to introduce LBM in detail in this paper. The paper structure is as follows:

1. **Lattice boltzmann method**; Show the governing equations and provide pseudocodes to promote the understandings
2. **Numerical results**[1]: Provide how we can validate the implementations, and how effective the parallel computation is

All the codes follow the pep8 style [2] and are tested using unittest[3]. Furthermore, **the step-by-step reproduction instruction is available** in `README.md` on this repository.

[1] The code is available at: https://github.com/nabenabe0928/high-performance-computing-fluid-dynamics-with-python

[2] https://www.python.org/dev/peps/pep-0008/

[3] https://docs.python.org/3/library/unittest.html

2

Lattice Boltzmann method

In this chapter, we describe how the equations used in LBM are derived. More specifically, we explain **Boltzmann transport equation (BTE)** [5], i.e. the basic equations of the kinetic theory of gases and how to handle the boundary conditions.

2.1 The Boltzmann transport equation (BTE)

The BTE formulates the time evolution of the particle probability density $f(\boldsymbol{x}, \boldsymbol{u}, t)$ given the velocity $\boldsymbol{u}$ and the position $\boldsymbol{x}$ of particles. The BTE relaxes the particle distribution to the Maxwell velocity distribution function [3] and the approximation of the relaxation of f towards f^{eq} is described as follows [6]:

$$\frac{df(\boldsymbol{x}, \boldsymbol{u}, t)}{dt} = -\frac{f(\boldsymbol{x}, \boldsymbol{u}, t) - f^{\mathrm{eq}}(\boldsymbol{u}; \rho(\boldsymbol{x}, t), \boldsymbol{u}(\boldsymbol{x}, t), T(\boldsymbol{x}, t))}{\tau} \tag{2.1}$$

where f^{eq} is statistical equilibrium, $T(\boldsymbol{x}, t)$ is the temperature at $\boldsymbol{x}$ of time step t and τ is a characteristic time. The characteristic time determines how quickly the fluid converges towards the equilibrium. The higher τ yields the slower convergence towards the equilibrium. Eq (2.1) is used for the update of the particle probability density function. Furthermore, this particle probability density function $f(\boldsymbol{x}, \boldsymbol{u}, t)$ is used for computing the physical states of the fluid, such as density and velocity. The momentum updates are performed via [7]:

$$\rho(\boldsymbol{x}, t) = \int f(\boldsymbol{x}, \boldsymbol{u}, t) d\boldsymbol{u} \tag{2.2}$$

$$\boldsymbol{u}(\boldsymbol{x}, t) = \frac{1}{\rho(\boldsymbol{x}, t)} \int \boldsymbol{u} f(\boldsymbol{x}, \boldsymbol{u}, t) d\boldsymbol{u} \tag{2.3}$$

The underlying equations allow to simulate fluid flow as seen in the latter parts of this paper.

2.2 Time-step update of the BTE

The aforementioned BTE is formulated in the continuous domain; therefore, we need to discretize sptially and temporally to make the computation feasible by simulations. In this paper, we focus on the discretization in the two dimensional space. The discretization for the space and time is performed so that the equality condition of the following inequality (Courant-Friedrichs-Lewy condition) holds [8, 9]:

$$\boldsymbol{c}_i \Delta t \leq ||\Delta \boldsymbol{x}_i|| \tag{2.4}$$

where Δt is the time step size and $\Delta \boldsymbol{x}_i$ is the distance between the closest grid in the direction of $\boldsymbol{c}_i$ that is defined:

$$\boldsymbol{c} = \begin{bmatrix} 0 & 1 & 0 & -1 & 0 & 1 & -1 & -1 & 1 \\ 0 & 0 & 1 & 0 & -1 & 1 & 1 & -1 & -1 \end{bmatrix}^\top \tag{2.5}$$

Note that this specific discretization in two-dimensional space with nine direction shown in Figure 2.1 is called D2Q9. In this setting, we first discretize the particle probability density function in nine directions by subscripting as $f_i(\boldsymbol{x}, t)$. Then Eq (2.2), (2.3) become the follwoings:

$$\rho(\boldsymbol{x}, t) = \sum_i f_i(\boldsymbol{x}, t) \tag{2.6}$$

$$\boldsymbol{u}(\boldsymbol{x}, t) = \frac{1}{\rho(\boldsymbol{x}, t)} \sum_i \boldsymbol{c}_i f_i(\boldsymbol{x}) \tag{2.7}$$

Note that we regard the density as unit molecular mass in Eq (2.6). Additionally, the equilibrium in Eq (2.1) is computed as:

$$\underbrace{f_i(\boldsymbol{x} + \boldsymbol{c}_i \Delta t, t + \Delta t) - f_i(\boldsymbol{x}, t)}_{\text{streaming}} = \underbrace{-\omega \Big[f_i(\boldsymbol{x}, t) - f_i^{\text{eq}}(\boldsymbol{x}, t) \Big]}_{\text{collision}} \tag{2.8}$$

where $\omega = \Delta t / \tau$ is the relaxation parameter. The equilibrium is computed as [10]:

$$f_i^{\text{eq}}(\boldsymbol{x}, t) = w_i \rho(\boldsymbol{x}, t) \Big[1 + 3\boldsymbol{c}_i \cdot \boldsymbol{u}(\boldsymbol{x}, t) + \frac{9}{2} (\boldsymbol{c}_i \cdot \boldsymbol{u}(\boldsymbol{x}, t))^2 - \frac{3}{2} ||\boldsymbol{u}(\boldsymbol{x}, t)||^2 \Big] \tag{2.9}$$

where the index i corresponds to Figure 2.1 and the weights are

$$w_i = \begin{cases} \frac{4}{9} & (i = 0) \\ \frac{1}{9} & (i = 1, 2, 3, 4) \\ \frac{1}{36} & (i = 5, 6, 7, 8) \end{cases} \tag{2.10}$$

In the streaming step, the grid receives the particle flow $f_i(\boldsymbol{x} + \boldsymbol{c}_i \Delta t, \cdot)$ from its nine adjacent grids. In the collision step, we relax the probability density function towards the equilibrium f_i^{eq} by considering the effects of the particle collision.

2.3 Boundary handling

In this section, we briefly discuss how we handle the particles that bump into boundaries. Note that the boundary handling is performed after the streaming step that is discussed in the previous section and we usually use the direction that is opposite to the direction i for the bounce back. For this reason, we will denote $f_i^\star$ as the i-th direction particle probability density function after the streaming step and $i^\star$ as the direction opposite, i.e. **reflected direction**, to i. Those directions follow D2Q9 illustrated in Figure 2.1. Additionally, there are the following two ways to implement the boundary conditions [11]:

1. **Dry nodes**: The boundaries are located on the link between nodes
2. **Wet nodes**: The boundaries are located on the lattice nodes

Since the boundary handling will be tedious when the boundaries are placed on the lattice nodes, and this is the case for wet nodes, we use **dry nodes** for the implementation.

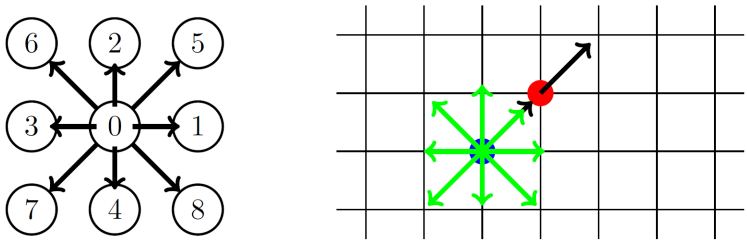

(a) (b)

Figure 2.1: (a) The discretization on the velocity space according to D2Q9. (b) The uniform two-dimensional grids for the discretization in the physical space.

2.3.1 Bounce-back from objects

The most basic boundary condition is **rigid wall** or the **bounce-back boundary condition**. In this condition, we apply the process without slip condition at the boundary. The equation at the boundary is computed as [12]:

$$f_i(\boldsymbol{x}_b, t + \Delta t) = f^\star_{i^\star}(\boldsymbol{x}_b, t) \tag{2.11}$$

When the **boundary moves** with the velocity of $\boldsymbol{U}_w$, the variation in the momentum of particles must be taken into consideration and the equation is modified as follows [12]:

$$f_i(\boldsymbol{x}_b, t + \Delta t) = f^\star_{i^\star}(\boldsymbol{x}_b, t) - 2w_i\rho_w \frac{\boldsymbol{c}_i \cdot \boldsymbol{U}_w}{c_s^2} \tag{2.12}$$

where c_s is the speed of sound and ρ_w is the density at the wall. The computation of ρ_w is usually performed by either of the followings [13, 14]:

1. Take the average density $\bar{\rho}$ of the simulated field
2. Extrapolate ρ_w using the particle probability density function in the physical domain

For the simplicity, we **take the first solution**.

2.3.2 Periodic boundary conditions (PBC)

In this section, we assume that we have boundary at $x = 0$ (inlet), $X - 1$ (outlet) where X is the number of the lattice grid in the x-axis. The most basic PBC assumes that the flow from outlet comes in from inlet as follows [12]:

$$f((0, y), t) = f((X - 1, y), t) \tag{2.13}$$

This condition is implicitly implemented during the streaming operation. Another PBC handles the pressure variation Δp between inlet and outlet. Since the density ρ is computed using the pressure p as $\rho = \frac{p}{c_s^2}$ where c_s is the speed of sound, the density at the inlet ρ_{in} and that at the outlet ρ_{out} can be computed accordingly given the constant pressure p_{out} at the outlet. Then the particle probability density functions at the inlet and the outlet are computed as follows [12]:

$$\begin{aligned} f_i^\star(0, y, t) &= f_i^{\text{eq}}(\rho_{\text{in}}, \boldsymbol{u}(X - 1, y, t)) + (f_i^\star(X - 1, y, t) - f_i^{\text{eq}}(X - 1, y, t)) \\ f_i^\star(X - 1, y, t) &= f_i^{\text{eq}}(\rho_{\text{out}}, \boldsymbol{u}(0, y, t)) + (f_i^\star(0, y, t) - f_i^{\text{eq}}(0, y, t)) \end{aligned} \tag{2.14}$$

3

Implementation

In this chapter, we describe how the LBM is implemented in Python and how to compute the LBM in parallel. All the implementation is assuming that the physical domain is discretized by D2Q9 and the horizontal axis is x and the vertical axis is y, respectively. Note that entire codes are based on Numpy[1] and mpi4py[2]. Throughout the chapter, `numpy` is imported as `np`.

3.1 Main routine

Algorithm 1 shows the pseudocode of the main processing in the LBM. Recall that $f(\cdot, t)$.shape $= (X, Y, 9)$, $\rho(\cdot, 0)$.shape $= (X, Y)$ and $\boldsymbol{u}(\cdot, 0)$.shape $= (X, Y, 2)$. First, we provide the initial values for the density and the velocity. Then, we compute the probability function and equillibrium and apply the collision step. The equillibrium implementation is shown in Algorithm 2. After applying equillibrium, we perform streaming operation shown in Algorithm 3 and slide each quantity to the adjacent cells. Finally, we apply the boundary handling at each boundary cell as described in Algorithm 4 and update the density and the velocity as in Eq 2.6, 2.7. Note that the order of each step might vary depending on literature [2, 12]. Additionally, we use as much slicing as possible in the Algorithms in order to speed up the runtime.

The Algorithm 3 uses the `np.roll` operation that enables to handle periodic boundary conditions automatically. This function rolls the array in the following manner:

$$\begin{aligned} \text{np.roll}(f[x][y][i], \text{shift} = \boldsymbol{c}_i, \text{axis} = (0, 1)) = f[nx][ny][i] \\ \text{where } nx = (x + \boldsymbol{c}_i[0])\%X, ny = (y + \boldsymbol{c}_i[1])\%Y \end{aligned} \tag{3.1}$$

where i is the direction index in D2Q9 and $\boldsymbol{c}_i$ is the vector that specifies the i-th direction in D2Q9. In the Algorithm 4, we use boolean matrices `in_boundary` and `out_boundary` that have the shape of $(X, Y, 9)$ so that we can refer to only elements that have bounce back or collision with the boundary. Additionally, we compute ρ_w by the average density [14]. Note that the domain is extended with virtual nodes at both edges of the periodic boundary in the PBC with pressure variation so that the implementation is more straightforward.

3.2 Parallel computation by MPI

In order to process the LBM in parallel, we employ the spatial domain decomposition and the messaging passing interface (MPI) so that we can compute collision step of the LBM in

[1]Numpy: https://numpy.org/
[2]mpi4py: https://mpi4py.readthedocs.io/en/stable/

Algorithm 1 The main routine of the lattice Boltzmann method

The grid size: X, Y, Relaxation factor : ω, Initial velocity: $\boldsymbol{u}_0$, Initial density: ρ_0 ▷ Inputs
Boundary conditions
function LATTICE BOLTZMANN METHOD
  $\rho(\boldsymbol{x}, 0) = \rho_0, \boldsymbol{u}(\boldsymbol{x}, 0) = \boldsymbol{u}_0$ for all $\boldsymbol{x} \in [0, X) \times [0, Y)$
  for $t = 0, 1, \ldots$ **do**
    $f^{\text{eq}}(\cdot, t) = \text{equillibrium}(\rho(\cdot, t), \boldsymbol{u}(\cdot, t))$ ▷ Eq (2.9)
    $f^{\star} = f + \omega(f^{\text{eq}} - f)$ ▷ Eq (2.8)
    $f^{\star}(\cdot, t) =$streaming$(f^{\star}(\cdot, t))$ ▷ Eq (2.8)
    $f(\cdot, t+1) =$ boundary_handling$(f^{\star}(\cdot, t), f^{\text{eq}}(\cdot, t))$ ▷ Eq (2.11), (2.12), (2.14)
    $\rho(\cdot, t+1), \boldsymbol{u}(\cdot, t+1)$=moments_update$(f(\cdot, t+1))$ ▷ Eq (2.6), (2.7)

Algorithm 2 Equillibrium

$\boldsymbol{w} =$ np.array$([\frac{4}{9}, \frac{1}{9}, \frac{1}{9}, \frac{1}{9}, \frac{1}{9}, \frac{1}{36}, \frac{1}{36}, \frac{1}{36}, \frac{1}{36}])$, $\boldsymbol{c}$ in Eq (2.5)
function EQUILLIBRIUM($\rho = \rho(\cdot, t)$, $\boldsymbol{u} = \boldsymbol{u}(\cdot, t)$) ▷ $\boldsymbol{u}$.shape $= (X, Y, 2)$, ρ.shape $= (X, Y)$
  u_norm2 = ($\boldsymbol{u}$ ** 2).sum(axis=-1)[..., None]
  u_at_c = $\boldsymbol{u}$ @ $\boldsymbol{c}^{\top}$ ▷ u_at_c.shape $= (X, Y, 9)$
  w_tmp, ρ_tmp = $\boldsymbol{w}$[None, None, ...], ρ[..., None] ▷ Adapt the shapes to u_at_c
  f^{eq} = w_tmp * ρ_tmp * (1 + 3 * u_at_c + 4.5 * (u_at_c) ** 2)-1.5 * u_norm2
  return f^{eq}

parallel. This is possible because the collision step does not require any communication between processes [15]. Then, we explain how we divide the domain. Suppose we are provided the number of processes of P, we first factorize P such that $P = P_0 \times P_1$ where $P_0, P_1 \in \mathbb{Z}^+$ and $P_0, P_1 = \arg\min_{P_0, P_1}(||P_1 - P_0||)$. Then, we divide the x-axis into P_0 intervals and y-axis into P_1 intervals where any pairs of intervals I_i, I_j in the same direction satisfy $-1 \leq ||I_i|| - ||I_j|| \leq 1$. Note that $||I||$ is the size of the interval I. This split of the domain achieves the most balanced distribution of the computation. For the streaming step, we need to consider particles moving from one process to another. We implement it using so-called **ghost cells** around the actual computational domain. Figure 3.1 shows the conceptual visualization of how each process communicates and ghost cells work. Since each process requires the four edges of adjacent processes, the commnications are required four times for each process. The Algorithm 5 shows the implementation using mpi4py. `grid_manager` is our self-developed module that allows to get useful information related to process location, the adjacent relation and so on. `Sendrecv` function is used for the commnication and each process receives an array from `dest` that is sent

Algorithm 3 Streaming operation

$\boldsymbol{c}$ in Eq (2.5)
function STREAMING($f^{\star} = f^{\star}(\cdot, t)$)
  f^{post} = np.zeros_like($f^{\star}$)
  for $i = 0, 1, \ldots, 8$ **do**
    f^{post}[..., i]=np.roll($f^{\star}$[..., i], shift=$\boldsymbol{c}_i$, axis=(0, 1)) ▷ Slide $f^{\star}$ one step to c[i]
  return f^{post}

Algorithm 4 Boundary conditions

Boolean matrix that represents where we have the bounce back: in_boundary
Boolean matrix that represents where we have the collision: out_boundary
The indices in D2Q9 s.t. the flow comes in given boundaries: in_indices
The indices in D2Q9 s.t. the flow goes out given boundaries: out_indices

function BOUNDARY HANDLLING($f^\star = f^\star(\cdot, t)$, $f^{\mathrm{eq}} = f^{\mathrm{eq}}(\cdot, t)$)
  if Rigid wall **then**
    f[in_boundary] = $f^\star$[out_boundary]
  if Moving wall **then**
    coef = np.zeros_like(out_boundary)
    for out_idx, ci, wi in zip(out_indices, c, w) **do**
      coef[:, :, out_idx] = 2 * wi * (ci @ $\boldsymbol{U}_w$) / c_s ** 2
    f[in_boundary] = $f^\star$[out_boundary]-ρ_w[out_boundary] * coef[out_boundary]
  if PBC with pressure variation **then** ▷ fluid flows from $x = 0$ to $X - 1$
    $f^{\mathrm{eq}}_{\mathrm{in}}, f^{\mathrm{eq}}_{\mathrm{out}}$ = equilibrium(ρ_{in}, $\boldsymbol{u}$[-2]), equilibrium(ρ_{out}, $\boldsymbol{u}$[1])
    f^{post}[0][:,out_indices]=$f^{\mathrm{eq}}_{\mathrm{in}}$[:,out_indices]+($f$[-2][:,out_indices]-$f^{\mathrm{eq}}$[-2][:,out_indices])
    f^{post}[-1][:, in_indices]=$f^{\mathrm{eq}}_{\mathrm{out}}$[:, in_indices]+($f$[1][:, in_indices] - f^{eq}[1][:, in_indices])
  return f

by `neighbor` and sends an array `sendbuf` to `neighbor`. Note that `buf` is the abbreviation of buffer and it is literally used for the buffer to communicate data.

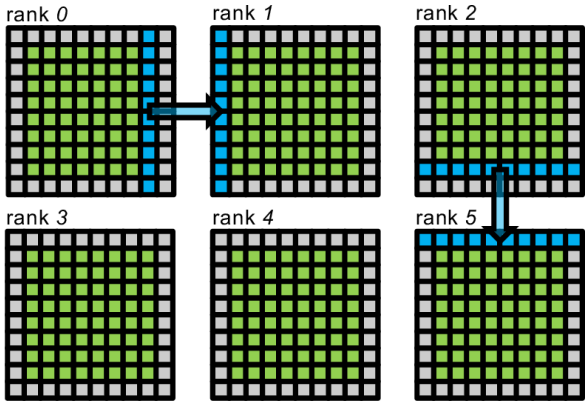

Figure 3.1: Domain decomposition and communication strategy in MPI. As described in the main text, we first divide each axis into P_0 and P_1 intervals and divide by the intervals. Each rank has green lattice points and this area is the active physical domain. Then we add an additional ghost cells for buffer (gray lattice points). During each communication step, the outermost green active lattice sends the data to the adjacent outermost ghost lattice (blue arrows). The figure is cited from Figure 2 in [15].

Algorithm 5 The communication of the particle probability density function

```
Process and lattice grids management: grid_manager
function COMMUNICATION
    for dir in grid_manager.neighbor_directions do          ▷ Iterate over the D2Q9 index
        dx, dy = c_i
        sendidx = grid_manager.step_to_idx(dx, dy, send=True)
        recvidx = grid_manager.step_to_idx(dx, dy, send=False)
        neighbor = grid_manager.get_neighbor_rank(dir)
        if dx == 0 then                                     ▷ send to top and bottom
            sendbuf = f[:, sendidx, ...].copy()
            grid_manager.rank_grid.Sendrecv(sendbuf=sendbuf, dest=neighbor,
                                            recvbuf=recvbuf, source=neighbor)
            f[:, recvidx, ...] = recvbuf
        else if dy == 0 then                                ▷ send to left and right
            sendbuf = f[sendidx, ...].copy()
            grid_manager.rank_grid.Sendrecv(sendbuf=sendbuf, dest=neighbor,
                                            recvbuf=recvbuf, source=neighbor)
            f[recvidx, ...] = recvbuf
    return f
```

4

Numerical results

In the previous chapter, we discuss the implementation details and how we implement and apply LBM to various settings. In this chapter, we show the visualizations and numerical results obtained from the series experiments.

4.1 Validation experiments

In the physics simulation, it is always important to validate whether the implementation is correct. Therefore, we first show how to validate the implementation using several examples.

4.1.1 Shear wave decay

The shear wave decay represents the time evolution of a velocity perturbation in the flow. Since the viscosity decays the velocity of the flow, the velocity converges to zero in the end. When we set the following sinusoidal perturbation in the velocity as the initial condition:

$$\boldsymbol{u}(\boldsymbol{x}, t=0) = \begin{bmatrix} u_x(y, t=0) \\ 0 \end{bmatrix} = \begin{bmatrix} \epsilon \sin \frac{2\pi y}{Y} \\ 0 \end{bmatrix} \tag{4.1}$$

Then the analytical solution for the time evolution of the velocity is calculated as follows [16]:

$$u_x(y,t) = \epsilon \exp\left(-\nu \left(\frac{2\pi}{Y}\right)^2 t\right) \sin \frac{2\pi y}{Y} \tag{4.2}$$

Note that this result is obtained using Navier-Stokes equations for incompressible fluid and the assumptions that the pressure term ∇p and the convection term $(\boldsymbol{u} \cdot \nabla)\boldsymbol{u}$ are negligible compared to the viscosity term $\nu \nabla^2 \boldsymbol{u}$. In Figure 4.1, we show the plot of both simulated results and the analytical solutions of sinusoidal velocity. Note that the initial condition follows Eq (4.1). As seen in the figure, the simulated results and the analytical solutions **perfectly fit** and thus we could validate our implementation of rigid wall and moments updates. Figure 4.2 shows the density distribution over time. This simulation uses the sinusoidal density in x-direction:

$$\rho(\boldsymbol{x}, 0) = \rho_0 + \epsilon \sin \frac{2\pi x}{X} \tag{4.3}$$

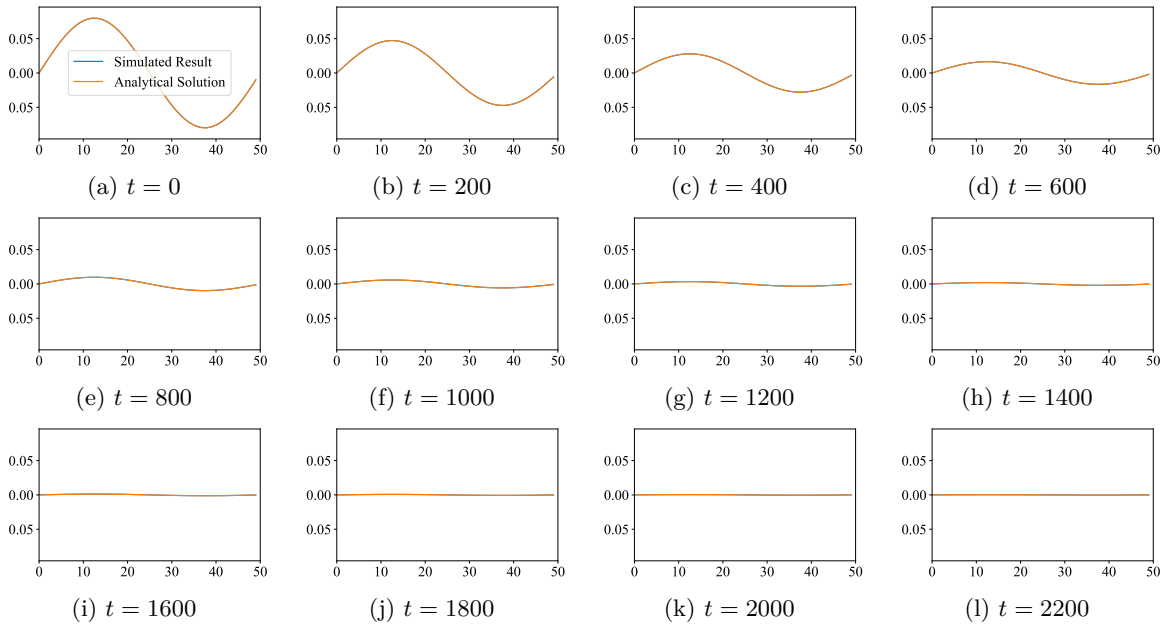

(a) $t = 0$ (b) $t = 200$ (c) $t = 400$ (d) $t = 600$

(e) $t = 800$ (f) $t = 1000$ (g) $t = 1200$ (h) $t = 1400$

(i) $t = 1600$ (j) $t = 1800$ (k) $t = 2000$ (l) $t = 2200$

Figure 4.1: The velocity evolution for the sinusoidal velocity at the $x = 25$ in the lattice grid size of $(50, 50)$. The x-axis shows the location in the y direction and the y-axis shows the magnitude of velocity at the corresponding location. The coefficients ϵ and the initial density ρ_0 are set to 0.08 and 1.0 respectively. The relaxation term ω are set to 1.0.

Additionally, we obtain the following equation regarding the viscosity by transforming Eq (4.2):

$$\begin{aligned} u_x(y,t) = \epsilon \exp\left(-\nu\left(\frac{2\pi}{Y}\right)^2 t\right) \iff \frac{u_x(y,t)}{\epsilon \sin\frac{2\pi y}{Y}} &= \exp\left(-\nu\left(\frac{2\pi}{Y}\right)^2 t\right) \\ -\nu\left(\frac{2\pi}{Y}\right)^2 t &= \log\frac{u_x(y,t)}{\epsilon \sin\frac{2\pi y}{Y}} \text{ (Take log of both sides)} \\ \nu &= -\frac{1}{t}\left(\frac{Y}{2\pi}\right)^2 \log\frac{u_x(y,t)}{\epsilon \sin\frac{2\pi y}{Y}} \end{aligned} \tag{4.4}$$

Note that we assume that $\epsilon \sin\frac{2\pi y}{Y} \neq 0$ and the assumptions for Eq (4.2) hold. We perform the experiments to validate Eq (4.4) using the exact experiment settings for Figure 4.1 and Figure 4.2 except the relaxation term ω. Note that the viscosity is computed as $\nu = \frac{1}{3}(\frac{1}{\omega} - \frac{1}{2})$. The results are shown in Figure 4.3. Based on the results, smaller and larger ω lead to numerical instability. Otherwise, the simulated results and analytical solution fit perfectly. Therefore, we need to avoid using ω closer to 0 or 2 for more accurate results.

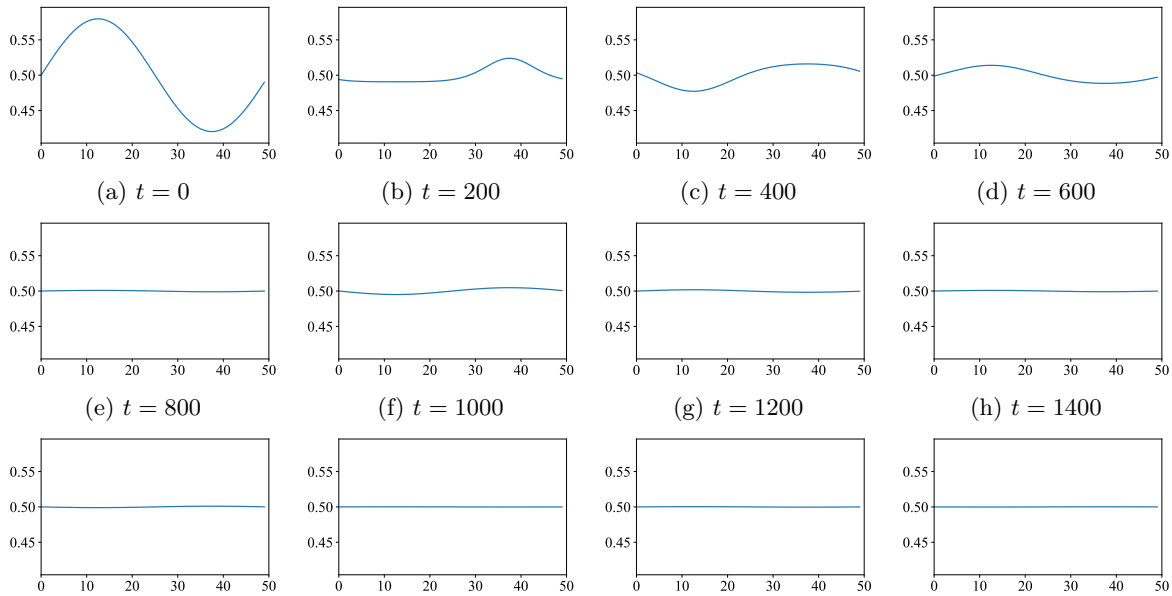

(a) $t = 0$ (b) $t = 200$ (c) $t = 400$ (d) $t = 600$

(e) $t = 800$ (f) $t = 1000$ (g) $t = 1200$ (h) $t = 1400$

(i) $t = 1600$ (j) $t = 1800$ (k) $t = 2000$ (l) $t = 2200$

Figure 4.2: The density evolution for the sinusoidal density at the $Y = 25$ in the lattice grid size of $(50, 50)$. The x-axis shows the location in the x direction and the y-axis shows the magnitude of density at the corresponding location. The coefficients ϵ and ρ_0 are set to 0.08 and 0.5 respectively. The relaxation term ω are set to 1.0.

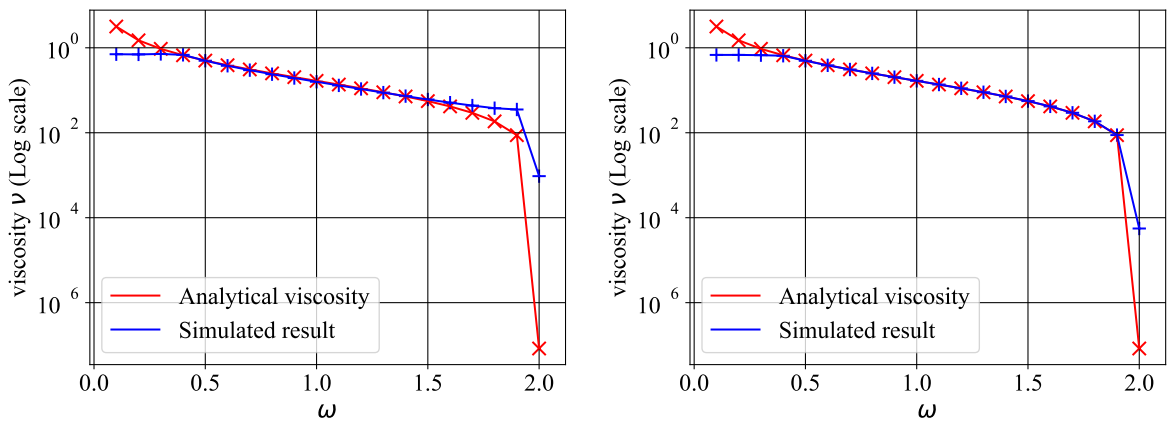

(a) Sinusoidal density (b) Sinusoidal velocity

Figure 4.3: The simulated viscosity value over various relaxation values ω. The analytical solution uses $\nu = \frac{1}{3}(\frac{1}{\omega} - \frac{1}{2})$ and the simulated result uses Eq (4.4). For the simulated results, we take the results at $t = 3000$ and compute the average of ν at $X = 25$ over the y-axis. Note that (a) uses the same parameters as in Figure 4.2 and (a) uses the same parameters as in Figure 4.1.

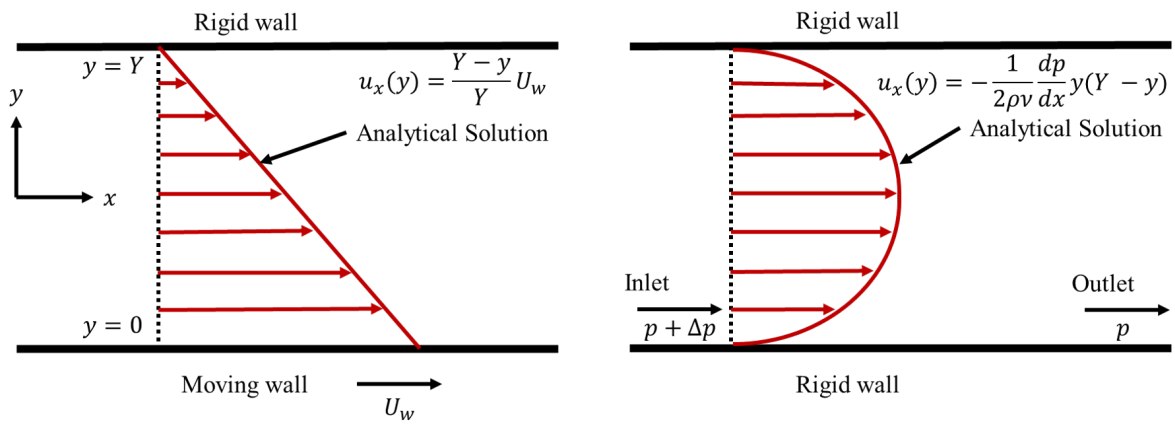

Figure 4.4: The conceptual visualizations of the Couette flow (Left) and Poiseuille flow (Right).

4.1.2 Couette flow

The Couette flow is the flow between two walls as shown in Figure 4.4: One is fixed and the other moves horizontally with the velocity of U_w. The flow is caused by the viscous drag force acting on the fluid. Since the Couette flow also has an analytical solution, we can validate the implementation of the moving wall. The analytical solution for Figure 4.4 is given by [17]:

$$u_x(y) = \frac{Y-y}{Y} U_w \tag{4.5}$$

where Y is the distance between the two walls and $u_x(y)$ is the horizontal velocity of the flow at the location of y. In the experiment, we apply the bounce-back boundary condition at the moving wall and the rigid wall and the periodic boundary conditions at the inlet and outlet. The results are shown in Figure 4.5. As shown in the figures, the flow velocity iteratively approaches the analytical solution and it perfectly fits in the end and the velocity stops growing as seen at $t = 1600, 2000$. From this experiment, the moving wall can be validated.

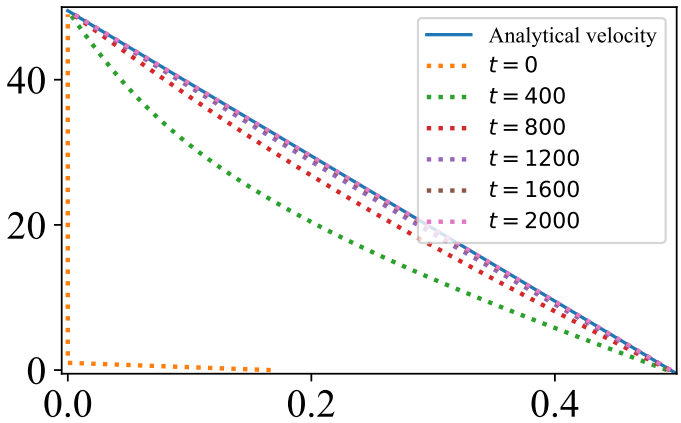

Figure 4.5: The velocity evolution at the $x = 25$ in the lattice grid size of $(50, 50)$. The wall velocity U_w at the bottom and the relaxation term ω are set to 50 and 0.3 respectively. The initial density is $\rho(\boldsymbol{x}) = 1.0$ and the initial velocity is $\boldsymbol{u}(\boldsymbol{x}) = (0, 0)$.

4.1.3 Poiseuille flow

The Poiseuille flow is the flow between two non-moving walls as shown in Figure 4.4. The flow is caused by a constant pressure difference $\frac{dp}{dx}$ in the horizontal direction of the two walls. The Poiseuille flow also has the analytical solution and we can validate the implementation of the periodic boundary conditions with pressure variation. The analytical solution for Figure 4.4 is given by [18]:

$$u_x(y) = -\frac{1}{2\rho\nu}\frac{dp}{dx}y(Y-y) \tag{4.6}$$

In the experiment, we apply the bounce-back boundary condition at the moving wall and the rigid wall and the periodic boundary condition with pressure variation at the inlet and outlet. Figure 4.6 presents the results and the simulated results approaches the analytical solutions as in the Couette flow. In the end, it fits completely and the velocity stops growing as seen at $t = 4000, 5000$.

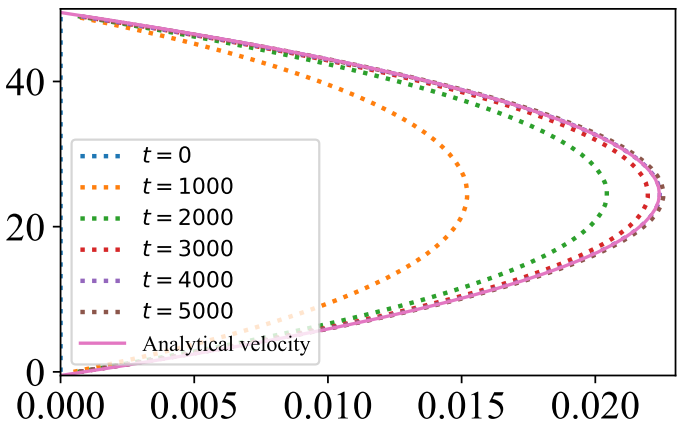

Figure 4.6: The velocity evolution at the $x = 25$ in the lattice grid size of $(50, 50)$. The relaxation term ω are is to 0.7. The density factor at the inlet and the density factor at the outlet are set to 0.3 and 0.301 respectively. The initial density is $\rho(\boldsymbol{x}) = 1.0$ and the initial velocity is $\boldsymbol{u}(\boldsymbol{x}) = (0, 0)$.

4.2 Lid-driven cavity

Finally, we handle a concrete example. In this paper, the lid-driven cavity shown in Figure 4.7 are simulated. The lid-driven cavity simulates the flow inside a box with three rigid walls and one moving wall, i.e. a lid. In this simulation, it is known that the turbulence is caused when the following Reynolds number is larger than 1000 [19]:

$$\mathrm{Re} = \frac{LU}{\nu} \tag{4.7}$$

where L is the characteristic length parameter of the body and U is the stream flow velocity. One key property of the Reynolds number is that two flow system is dynamically similar if the Reynolds number and the geometry are similar [20]. Therefore, we present the results with

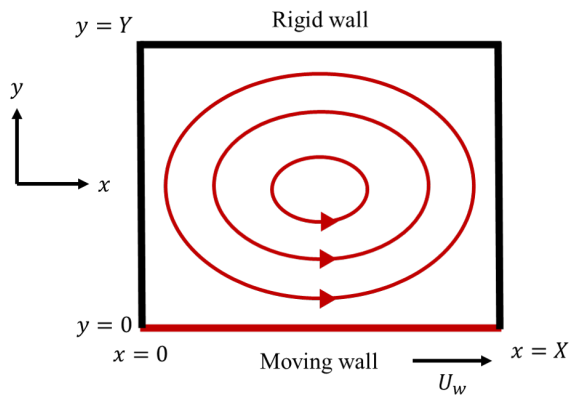

Figure 4.7: The conceptual visualizations of the lid-driven cavity.

various viscosity ν and the wall velocity $U = U_w$ that satisfy the Reynolds number of 1000 under $L = X = Y = 300$ in Figure 4.8. As the viscosity and velocity becomes larger, the convergence becomes quicker. On the other hand, all the settings converge to the similar flow in the end as indicated in the key property of the Reynolds number.

This experiment requires long time to complete. For example, it takes 1 hour to finish one simulation using intel core i7–10700 and 32GB RAM. Recall that the advantage of LBM is to allow us to compute the simulation in parallel easily. For this reason, we test the scalability of this simulation using various number of processes. Note that all the experiments related to the scaling test are performed on **BWUniCluster** [1]. The implementation follows Section 3.2. Figure 4.9 shows the plot of MLUPS, a.k.a. million lattice updates per second, and the number of processes. Ideally, the MLUPS grows linearly with respect to the number of processes. However, it does not happen because of the latency of the communication and the waiting for the synchronization as described in Amdahl's law [21]. Such slow down is also seen in Figure 4.9.

[1] https://wiki.bwhpc.de/e/Category:BwUniCluster_2.0

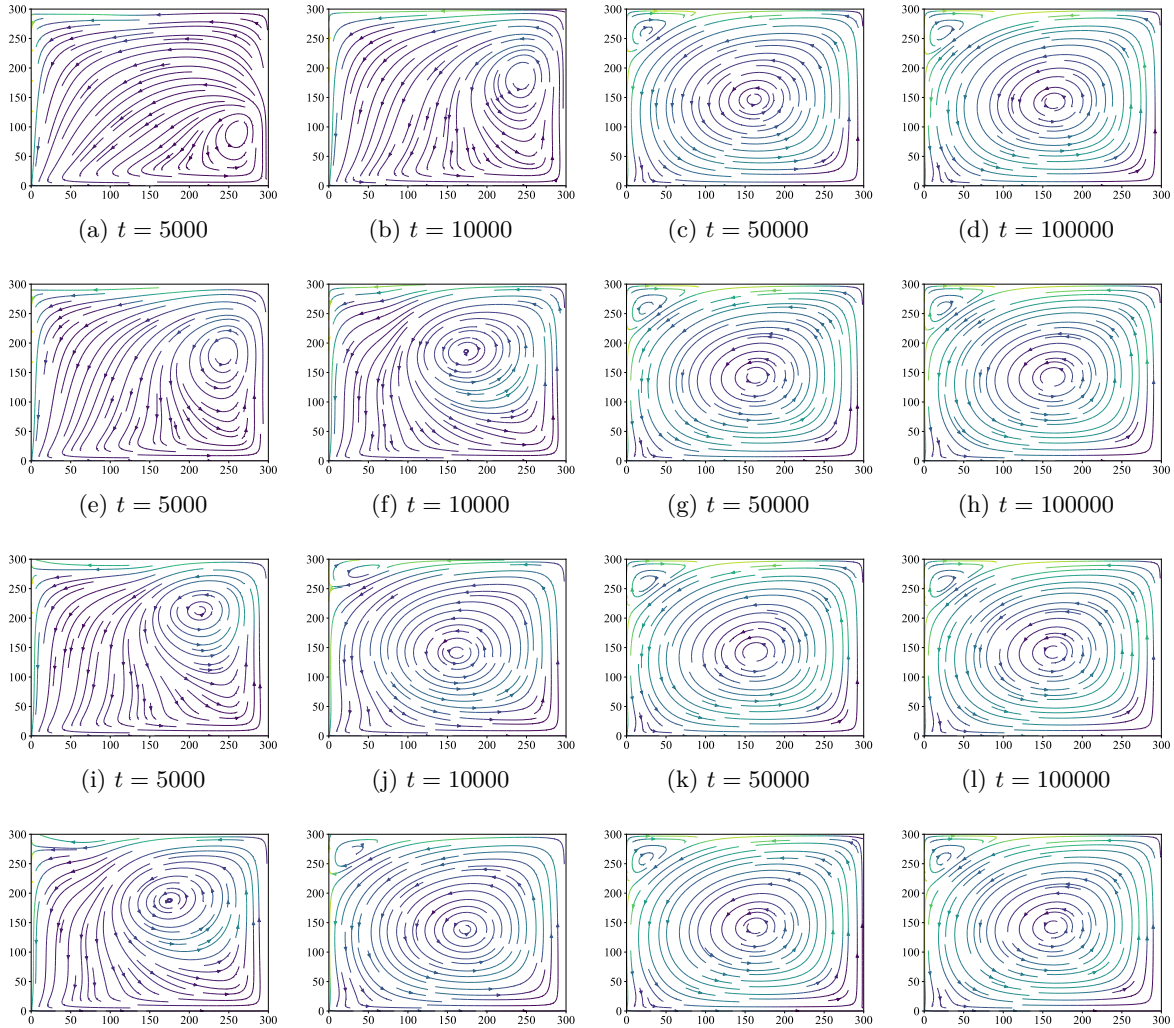

(a) $t = 5000$ (b) $t = 10000$ (c) $t = 50000$ (d) $t = 100000$

(e) $t = 5000$ (f) $t = 10000$ (g) $t = 50000$ (h) $t = 100000$

(i) $t = 5000$ (j) $t = 10000$ (k) $t = 50000$ (l) $t = 100000$

(m) $t = 5000$ (n) $t = 10000$ (o) $t = 50000$ (p) $t = 100000$

Figure 4.8: The stream plots of sliding lid with the lattice grid size of $(300, 300)$. Figure (a) – (d) are the results of the viscosity $\nu = 0.03$ and the wall velocity 0.1. Figure (e) – (h) are the results of the viscosity $\nu = 0.06$ and the wall velocity 0.2. Figure (i) – (l) are the results of the viscosity $\nu = 0.09$ and the wall velocity 0.3. Figure (m) – (p) are the results of the viscosity $\nu = 0.12$ and the wall velocity 0.4. Note that each setting is chosen to satisfy the Reynolds number 1000. The initial density is $\rho(\boldsymbol{x}) = 1.0$ and the initial velocity is $\boldsymbol{u}(\boldsymbol{x}) = (0, 0)$.

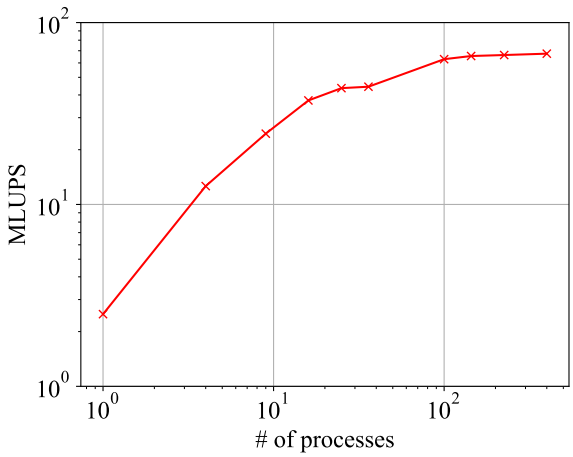

Figure 4.9: The scaling test of the sliding lid simulation. The grid size is 300×300. The number of processes are $1, 4, 9, 16, 25, 36, 100, 144, 225, 400$ respectively. Note that both axes are log-scale. The viscosity and the wall velocity are set to $\nu = 0.03$ and 0.1. The initial density is $\rho(\boldsymbol{x}) = 1.0$ and the initial velocity is $\boldsymbol{u}(\boldsymbol{x}) = (0, 0)$.

5

Conclusions

In this paper, we describe what the LBM is and how we implement it. Chapter 1 describes the motivation behind the numerical integrations and mentions the advantages of the LBM, i.e. simple implementation and the scalability with respect to the computational resources.

Chapter 2 explains the theoretical aspects of LBM and how those equations are pluged in the computational simulations. More specifically, the discretization of each equation and the boundary handlings are presented.

Chapter 3 shows the algorithms of each component. Especially, we focus on the descriptions how the simulation should be implemented using numpy which is effective to speed up Python implementations. Additionally, the MPI usage and the domain division method is described. Note that each algorithm in our implementation is tested using pytest and abstracted as much as possible so that each component can be reused and we can reduce the bugs over the whole implementations.

Chapter 4 presents the validations of each component using the comparison between the analytical solutions and visualizes how the LBM works in the lid-driven cavity example. For the validations, we use the shear wave decay, the Couette flow and the Poissuille flow and show the analytical solutions for each phenomenon. After the validations, we show the lid-driven cavity simulation exhibits the similar dynamics when we have a constant Reynolds number. Furthermore, we test the scalability of the LBM in the lid-driven cavity simulation and show about the 30 times speed up using 100 processes.

Bibliography

[1] Praveen Padagannavar and Manohara Bheemanna. Automotive computational fluid dynamics simulation of a car using ansys. International Journal of Mechanical Engineering and Technology (IJMET) Volume, 7:91–104, 2016.

[2] Krüger Timm, H Kusumaatmaja, A Kuzmin, O Shardt, G Silva, and E Viggen. The lattice Boltzmann method: principles and practice. Springer: Berlin, Germany, 2016.

[3] Kerson Huang. Statistical mechanics, john wily & sons. New York, page 10, 1963.

[4] D Raabe. Overview of the lattice boltzmann method for nano-and microscale fluid dynamics in materials science and engineering. Modelling and Simulation in Materials Science and Engineering, 12(6):R13, 2004.

[5] Guy R McNamara and Gianluigi Zanetti. Use of the boltzmann equation to simulate lattice-gas automata. Physical review letters, 61(20):2332, 1988.

[6] Prabhu Lal Bhatnagar, Eugene P Gross, and Max Krook. A model for collision processes in gases. i. small amplitude processes in charged and neutral one-component systems. Physical review, 94(3):511, 1954.

[7] B Caroli, C Caroli, and B Roulet. Non-equilibrium thermodynamics of the solidification problem. Journal of crystal growth, 66(3):575–585, 1984.

[8] Roger Peyret and Thomas D Taylor. Computational methods for fluid flow.

[9] James D Sterling and Shiyi Chen. Stability analysis of lattice boltzmann methods. Journal of Computational Physics, 123(1):196–206, 1996.

[10] Guo Zhao-Li, Zheng Chu-Guang, and Shi Bao-Chang. Non-equilibrium extrapolation method for velocity and pressure boundary conditions in the lattice boltzmann method. Chinese Physics, 11(4):366, 2002.

[11] H Liu and JG Zhou. Lattice boltzmann approach to simulating a wetting–drying front in shallow flows. Journal of fluid mechanics, 743:32–59, 2014.

[12] Sauro Succi. The lattice Boltzmann equation: for complex states of flowing matter. Oxford University Press, 2018.

[13] Qisu Zou and Xiaoyi He. On pressure and velocity boundary conditions for the lattice boltzmann bgk model. Physics of fluids, 9(6):1591–1598, 1997.

[14] Sorush Khajepor, Jing Cui, Marius Dewar, and Baixin Chen. A study of wall boundary conditions in pseudopotential lattice boltzmann models. Computers & Fluids, 193:103896, 2019.

[15] Lars Pastewka and Andreas Greiner. Hpc with python: An mpi-parallel implementation of the lattice boltzmann method. 2019.

[16] Linlin Fei, Kai H Luo, and Qing Li. Three-dimensional cascaded lattice boltzmann method: Improved implementation and consistent forcing scheme. Physical Review E, 97(5):053309, 2018.

[17] Péter Nagy-György and Csaba Hős. A graphical technique for solving the couette-poiseuille problem for generalized newtonian fluids. Periodica Polytechnica Chemical Engineering, 63(1):200–209, 2019.

[18] AA Mendiburu, LR Carrocci, and JA Carvalho. Analytical solution for transient onedimensional couette flow considering constant and time-dependent pressure gradients. Revista de Engenharia Térmica, 8(2):92–98, 2009.

[19] TP Chiang, WH Sheu, and Robert R Hwang. Effect of reynolds number on the eddy structure in a lid-driven cavity. International journal for numerical methods in fluids, 26(5):557–579, 1998.

[20] Pijush K Kundu, Ira M Cohen, and D Dowling. Fluid mechanics 4th, 2008.

[21] Gene M Amdahl. Validity of the single processor approach to achieving large scale computing capabilities. In Proceedings of the April 18-20, 1967, spring joint computer conference, pages 483–485, 1967.